Case Studies in Thermal Engineering 52 (2023) 103745

Contents lists available at ScienceDirect

Case Studies in Thermal Engineering

journal homepage: www.elsevier.com/locate/csite

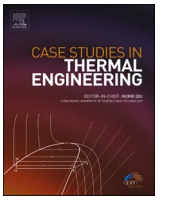

Energy performance analysis of a cascade heat pump system for heating in a semiconductor fabrication plant

Taek-Don Kwon [a,b], Woo-Hyun Jung [a], Jae-Weon Jeong [b,*]

[a] Division of Global Fabrication & Infra Technology, Samsung Electronics, Hwaseong-si, Gyeonggi-do, 18448, Republic of Korea
[b] Department of Architectural Engineering, College of Engineering, Hanyang University, Seoul, 04763, Republic of Korea

ARTICLE INFO

Handling Editor: Huihe Qiu

Keywords:
Semiconductor fabrication plant
Cascade cycle
Centrifugal heat pump
Outdoor air-conditioner
Heating equipment

ABSTRACT

To reduce carbon emissions, active research is being conducted on replacing the heating equipment using fossil fuels with heat pumps. While heat pumps still utilize electricity and have associated carbon emissions, they possess the potential to consistently decrease carbon emissions owing to the growing availability of renewable energy sources.

In this study, the applicability of a heat pump system capable of supplying 86 °C hot water for heating a semiconductor fabrication plant was verified. In addition, there are a few results considering the energy saving effect that can be obtained from the heat source. Therefore, reflecting the characteristics of a semiconductor fabrication plant, which requires a huge cooling load to remove heat from equipment even in winters, a cascade heat pump system using a chiller as a low-cycle heat pump was proposed. Compared to a boiler, the heat pump system has the advantage of reducing the load on the typical chiller system as it can supply cold and hot water.

On comparison, the cascade heat pump system, which incorporates the energy-saving effect derived from the heat source, demonstrated 66 % of primary energy and 56 % carbon emissions than the boiler. Consequently, the cascade heat pump outperformed the boiler system.

Nomenclature

V	volume [m^3]
$c_{p,sat}$	specific heat of saturated steam [= 1.805 kJ/kg °C]
c_p	specific heat at constant pressure [kJ/kg °C]
C	heat capacity rate [kW/K]
E	primary energy [kW]
h	enthalpy [kJ/kg]
h_w	vaporization enthalpy of water [= 2501 kJ/kg]
W	power consumption [kWh]
$\dot{m}$	mass flow rate [kg/s]
P	pressure [kPa]
Q	load [kW]
S	steam evaporation [kg/ Nm^3]

* Corresponding author.
E-mail address: jjwarc@hanyang.ac.kr (J.-W. Jeong).

https://doi.org/10.1016/j.csite.2023.103745
Received 7 September 2023; Received in revised form 6 November 2023; Accepted 9 November 2023
Available online 14 November 2023

T	temperature [°C]
HR	humidity Ratio [kg/kg]

Greek Symbols

ρ	density [kg/ m^3]
ε	effectiveness [%]

Subscripts

evap	evaporator
exp	expansion valve
c	cold fluid
comp	compressor
cond	condenser
cool	cooling
h	hot fluid
heat	heating
max	maximum
med	median
min	minimum
ref	refrigerant

Abbreviations

CCHPS	cascade heat pump system
CHW	chilled water
COP	coefficient of performance
C/C	cooling coil
CW	cooling water
FAB	semiconductor fabrication plant
H/C1	heating coil1
H/C2	heating coil2
HRC	heat recovery chiller
HCHP	high-cycle heat pump
LCHP	low-cycle heat pump
OAC	outdoor air-conditioner
PR	pressure ratio
PC/C	pre-cooling coil
PH/C	pre-heating coil
RH/C	reheating coil
WSS	water showering system

1. Introduction

The air temperature and humidity specification in the clean room of a semiconductor fabrication plant (FAB) is 23 °C, with a humidity ratio of 0.00733 kg/kg [1]. Therefore, in winter, cold air must be heated before being supplied to the clean room. In FAB, gas boilers are commonly used for heating. However, the boilers emit a large amount of carbon dioxide due to the burning of fossil fuels [2]. To solve this problem, alternative heating technologies that do not rely on fossil fuels, such as heat pumps, should be considered. Electricity is the primary form of energy derived from renewable energy sources [3], and literature indicates that the percentage of renewable energy production will rise [4–6]. Even using a heat pump with a coefficient of performance (COP) of over 3.5 that uses electricity supplied by thermal power rather than renewable energy can remove 34 % of carbon dioxide emitted by a gas-fired boiler [7]. Therefore, the conversion from boiler to heat pump is crucial.

Due to the huge heating demand, spatial limitation, the water-source centrifugal heat pump is mainly used in the industry [7]. The available heat sources for heat pumps in FAB include cooling water (CW) and return chilled water (CHW), with the maximum temperatures of 39 °C and 17 °C, respectively. The heat pump must supply hot water (HW) at a temperature above 80 °C to the heat sink.

Previous studies have been conducted on the water-source heat pump using various refrigerant cycle configurations (e.g., Refs. [8–14]). These studies can be classified into two main types: single-cycle and cascade-cycle. Hybrid methods also combine a stand-alone renewable energy system (e.g., photovoltaic/thermal, geothermal). However, most of them have only been studied as a general building application (see, e.g., Refs. [15–19]), thus, a hybrid method was excluded from the main ways.

Single-cycle heat pumps have one refrigerant cycle between the heat sink and the heat source. In Ref. [8], Jiang et al. studied the COP of the heat pump using the R-1233zd refrigerant that could supply HW above 80 °C with a heat source temperature over 30 °C. However, R-1233zd is not yet commonly utilized; thus, we searched the study results on the heat pump using the R-134a refrigerant,

which is the third most used refrigerant worldwide [20]. Liu et al. investigated a simulation logic to predict the COP of a heat pump using R-134a [9]. This heat pump could produce HW at 90 °C with a heat source temperature over 30 °C. The simulation logic accurately predicted the COP within the error range of 4.5–5.1 % when compared with the actual experimental results. Previous research also showed a disadvantage of a single cycle. In Ref. [10], the maximum PR of one-stage compressor on the market was limited to 2.5. To overcome this limitation, most single-cycle centrifugal heat pumps can have a maximum PR of 5.0 by adopting a two-stage compressor. Therefore, when considering a single-cycle heat pump using R-134a with an assumption of the approach temperature of 1 °C, the temperature of the heat source must be maintained above 23 °C to produce 80 °C HW within the PR range of 5.0.

Cascade-cycle heat pumps connect two single cycles using different refrigerants. Therefore, if the cascade-cycle employs two heat pumps with a two-stage compressor, the PR can exceed 5.0 [11–14]. In Ref. [11], Uusitalo et al. investigated the performance of the cascade cycle under conditions similar to the temperatures of the heat sink and heat source of the FAB. Despite the high PR, it was possible to operate the cascade-cycle heat pump system when using various refrigerants. Therefore, when producing HW at 80 °C or higher in FAB, return CHW can also be used as a heat source. However, single cycle is advantageous when the PR of the compressor is low due to the small temperature difference between the heat sink and the heat source [21].

Based on the literature review, single-cycle applications are suitable when using CW as the heat source in FAB, while cascade-cycle applications are necessary when using CHW as the heat source. However, notably, the CW is produced from a chiller, which cools CHW from 17 °C to 12 °C. Chiller and heat pump are equipment that operate on the same principle and have different names depending on whether the main purpose of use is CHW or HW production. Therefore, a chiller can be seen as a heat pump. Summarizing the above, when adopted with a heat pump that uses the CW as a heat source, a cascade-cycle heat pump system (CCHPS) is formed.

In this study, we considered a chiller as a low-cycle heat pump (LCHP) and analyzed the performance of a cascade cycle combining a high-cycle heat pump (HCHP) through simulation. Previous research on the heat pump cycle has primarily analyzed COP of EHP; however, the effects that can be obtained from the heat source have not been analyzed yet. Therefore, we checked the operating power of the chiller can be saved when CHW production is considered as the heat source of the CCHPS. The overall energy performance of the CCHPS, considering both the energy consumption of CCHPS and the energy savings of the chiller system was confirmed. Furthermore, by comparing CCHPS with a boiler, potential benefits of adopting the CCHPS was assessed. In this study, calculations and refrigerant properties were confirmed using the Engine Equation Solver program, excluding the TRNSYS simulation.

2. System overview

2.1. Outdoor air-conditioner

A large-scale OAC for a semiconductor cleanroom consists of four heating coils, two cooling coils, and two humidification devices.

In summers, pre-cooling coil (PC/C) and cooling coil (C/C) are used to cool and dehumidify hot and humid air. The cooled and dehumidified air passes through the water-showering system (WSS), where it undergoes partial humidification. Then, reheating coil (RH/C) reheats the air, considering the temperature rise caused by the heat generated by the fan and supplies the air to the cleanroom at a temperature of 15.5 °C and a humidity ratio of 0.00786 kg/kg (see Fig. 1).

In winters, pre-heating coil (PH/C), PC/C (w), heating coil1 (H/C1), and heating coil2 (H/C2) are used for the heating. PC/C (w) implies that PC/C is used for air heating in winter. PH/C is used to heat sub-zero outdoor air to a desirable temperature. To prevent freezing, an 80 °C antifreeze solution circulates inside the PH/C coil. PC/C (w) is used to reduce the heating load of H/C1 and the load on the chiller system by exchanging heat between the 12 °C CHW and induced air. H/C1 and H/C2 are used to increase the temperature of the air in front of the WSS, thereby improving the humidification efficiency. The H/C1 utilizes the 28 °C CW from the condenser of the chiller. H/C2 uses the HW at 80 °C. Humidification primarily occurs in the WSS installed to remove soluble gases from the air. To cope with rapid changes in the outdoor air humidity during transitional seasons, intermittent use of a steam humidifier is used, as shown in Fig. 2.

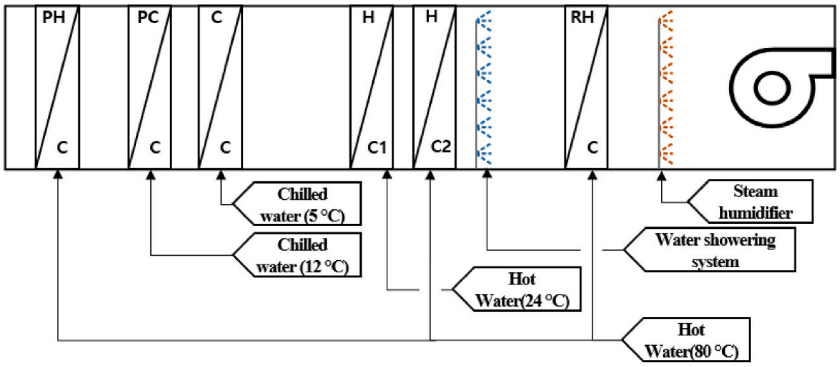

Fig. 1. Schematic of an outdoor air-conditioner for a cleanroom in Samsung Electronics.

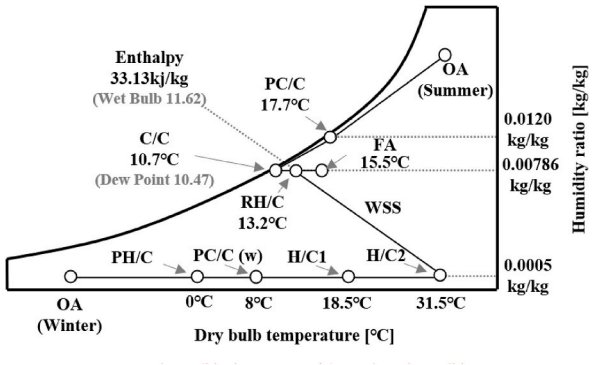

Fig. 2. Air-conditioning process of the outdoor air-conditioner.

2.2. Heat sources of the outdoor air-conditioner

2.2.1. Cascade heat pump system

Fig. 3 shows that the OAC installed in Samsung Electronics uses the boiler as the heating equipment. The steam is used to heat hot water2 (HW2) and antifreeze solution. H/C1 heats the air using hot water3 (HW3), which is heated by cooling water2 (CW2) from the heat recovery chiller (HRC).

In this study, the system was designed in such a way that the coils, originally receiving heat from the boiler, received heat from CCHPS. Meanwhile, H/C1 used CW2 to heat the air as in the present. Fig. 4 shows the OAC system with CCHPS. CCHPS, supplying hot water1 (HW1) to OAC, consists of two heat pumps and three pumps. The HCHP uses R-134a, and LCHP uses the R-123 refrigerant. Both heat pumps use centrifugal compressors.

In this study, the chiller was considered as an LCHP. When using the chiller as an LCHP, the cooling water1 (CW1) does not reach the cooling tower and is used as a heat source for the HCHP.

The HCHP produced HW1 at 86 °C, which exchanged heat with the fluid circulating through the OAC heating coil. Separate heat exchangers were used for the antifreeze solution circulating in PH/C and the water circulating in H/C2 and R/H to prevent mixing.

The total energy consumption of the CCHPS depended on the PR of the LCHP and HCHP. The temperature of HW1 supplied from the HCHP was fixed at 86 °C, and the temperature of CHW supplied from the LCHP was fixed at 12 °C. Therefore, the temperature of the CW1 circulating through the condenser of the LCHP and the evaporator of the HCHP became a variable in determining the PR of each heat pump. The energy consumption of the LCHP and HCHP was analyzed based on the temperature range setting for CW1, as shown in Fig. 5.

2.2.2. Steam boiler system

Currently, the OAC receives heat from the steam produced by the boiler. The boiler system is a reference system for analyzing the performance of CCHPS. The boiler system consists of a feed water pump, forced drift fan, main boiler, and economizer, as shown in Fig. 6.

The boiler is assumed to be a water tube type that uses city gas as fuel and produces 686.5 kPa (=7 kgf/cm^2) steam. At the desired site, 686.5 kPa steam is reduced to 196.1 kPa (=2 kgf/cm^2) for use, and the condensate generated after heat exchange is recovered to the feed water tank and reused. The water temperature of the feed water tank is assumed to be 60 °C, and the 85 °C feed water heat-exchanged with the exhaust gas in the economizer is sent to the drum. At this time, it is assumed that there is no heat loss and leakage

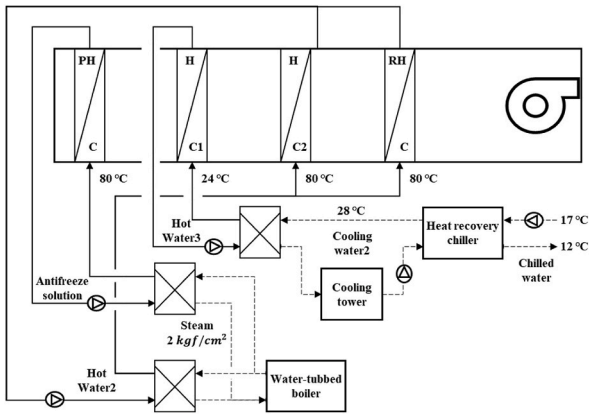

Fig. 3. Conventional heating system for the outdoor air-conditioner.

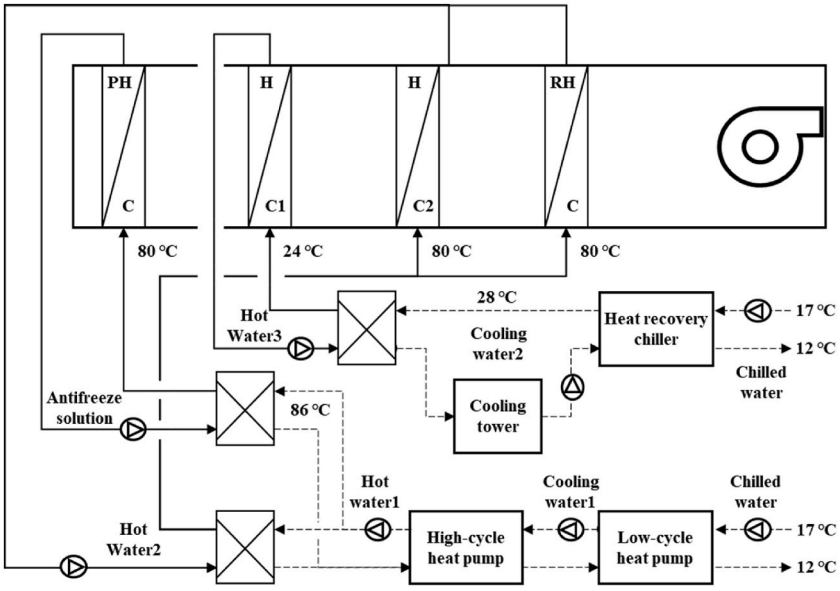

Fig. 4. Outdoor air-conditioner with cascade heat pump system for heating.

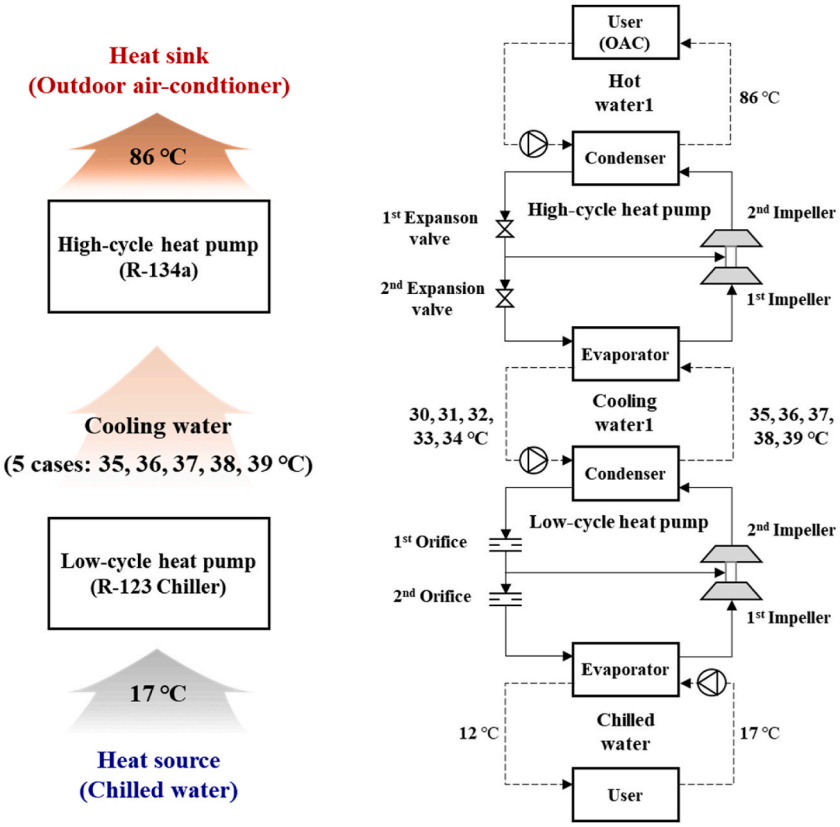

Fig. 5. Overview of the detailed configuration of the cascade heat pump system.

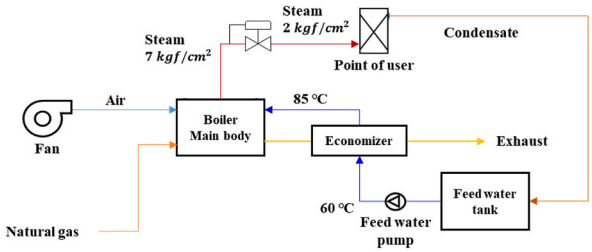

Fig. 6. Schematic of the boiler system configuration.

steam.

3. Simulation and theoretical modelling

3.1. TRNSYS model for estimating the heat load of the outdoor air-conditioner

To determine the annual load of the OAC, TRNSYS was used. The OAC were based on official meteorological data from the Suwon city, South Korea [22]. The study reflects outdoor air temperature and humidity conditions for 8760 h in Suwon city. The supply air volume of the OAC was set at 2000 m^3/min, with the final supply temperature and humidity conditions of 15.5 °C and 0.00786 kg/kg, respectively.

In the TRNSYS simulation, Type 670 was used for the heating coil, Type 508 for the cooling coil, and Type506 for the WSS. For the steam humidifier, as no suitable component was available, a calculator was used to input the relevant calculation formula. The main components used in the simulation are summarized in Table 1 [23]. The input conditions for the simulation are listed in Table 2. At this time, the specific heat of the antifreeze was assumed to be 40 % of ethylene glycol concentration at 82.2 °C (=180 °F) [24].

The coils in the OAC undergoes changes in heat exchange efficiency based on the temperature and flow rate of the supplied heat source. By modelling the Type 670 as the heating coil, it is possible to calculate and input the heat exchange efficiency, thus obtaining more accurate results. The Type 508, modeled as the cooling coil, incorporates a by-pass factor. The heat exchange efficiencies and by-pass factors for each coil are summarized in Table 3. The final schematic of the modeled OAC using TRNSYS is depicted in Fig. 7.

Specific set values and control logic were defined to ensure the desired temperature and humidity in the clean room, as shown in Table 4.

Eqs. (1) and (2) are used to heat the air in conditions where humidification is required during the winter and summer seasons.

$$T_{H/C1,set} = \frac{\left(33.13kJ/kg - h_w \times HR_{H/C1}\right)}{\left(c_{p,air} + c_{p,sat} \times HR_{H/C1}\right)} \tag{1}$$

$$T_{H/C2,set} = \frac{\left(33.13kJ/kg - h_w \times HR_{H/C2}\right)}{\left(c_{p,air} + c_{p,sat} \times HR_{H/C2}\right)} \tag{2}$$

To achieve humidification through WSS, it is necessary to heat the incoming air using the equipment. H/C1 and H/C2 play a role in heating the air to the specified enthalpy value. However, the components of H/C1 and H/C2 used in the TRNSYS simulation operate based on temperature set values. Therefore, it is necessary to convert the enthalpy set value into temperature. The enthalpy value is fixed at 33.13 kJ/kg, and equations (1) and (2) are used to calculate the temperature, considering the humidity ratio of the incoming air for H/C1 and H/C2.

Heating and humidification equations were used based on seasonal requirements. The simulation logic considered maximizing the heat transfer in H/C1 and H/C2 for efficient humidification. Finally, when the air passing through H/C2 is humidified to meet the

Table 1
List of main components in the TRNSYS simulation.

Components	TRNSYS type
Weather data input	Type 9
Psychrometric data file	Type 33
Heating coil	Type 670
Cooling coil	Type 508
Water showering system	Type 506
Fan	Type 642
Boiler	Type 638
Feed water pump	Type 110
Steam system control	Type 22
Steam flow diverter	Type 594
Plotter	Type 65
Printer	Type 45
Steam humidification	Calculator

Table 2
Parameters of the simulation conditions.

Weather data		Korea meteorological administration (2022, Suwon city)
Outdoor air-conditioner	Capacity of fan	2000 m^3/min
	Number of fans	1
	Total air flow	2000 m^3/min
Air properties	Density	1.2 kg/ m^3
	Specific heat	1.006 kJ/kgK
Water properties	Density	1000 kg/ m^3
	Specific heat	4.19 kJ/kgK
Antifreeze properties	Specific heat	3.66 kJ/kgK

Table 3
Coil effectiveness and the by-pass factor.

Coil	PH/C	PC/C (w)	H/C1	H/C2	RH/C	PC/C	C/C
Effectiveness	0.18	0.67	0.66	0.21	0.14	–	–
By-pass factor	–	–	–	–	–	0.15	0.15

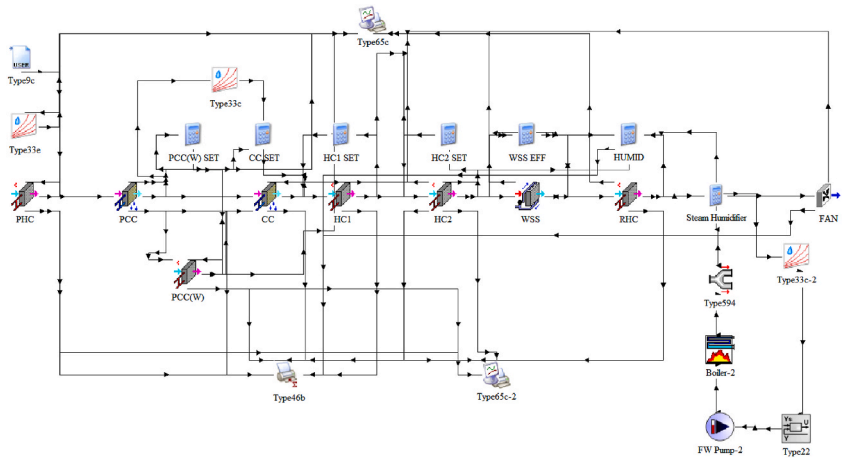

Fig. 7. Schematic of the TRNSYS simulation.

Table 4
Detailed operation logic for each component of the outdoor air-conditioner.

Components	Control logic	Set value
PH/C	outdoor air temp $\leq$ 0 °C; ON	0 °C
	outdoor air temp >0 °C; OFF	
PC/C (w)	inlet air temp $\leq$ 8 °C; ON	8 °C
	inlet air temp >8 °C; OFF	
PC/C	inlet air temp $\leq$ 17.7 °C; OFF	17.7 °C
	inlet air temp >17.7 °C; ON	
C/C	inlet air enthalpy $\leq$ 33.13 kJ/kg; OFF	Temp set: None
	inlet air enthalpy >33.13 kJ/kg; ON	Temp set: 10.47 °C
H/C1	inlet air humidity ratio <0.00786 kg/kg; ON	Temp set: Eq. (1)
	inlet air humidity ratio $\geq$ 0.00786 kg/kg; OFF	Temp set: 10.47 °C
H/C2	inlet air humidity ratio <0.00786 kg/kg; ON	Temp set: Eq. (2)
	inlet air humidity ratio $\geq$ 0.00786 kg/kg; OFF	Temp set: 10.47 °C
WSS	inlet air humidity ratio <0.00786 kg/kg; ON	Temp set: Eq. (3)
	inlet air humidity ratio $\geq$ 0.00786 kg/kg; OFF	Efficiency set: 92 %
RH/C	inlet air temp $\leq$ 13.2 °C; ON	13.2 °C
	inlet air temp >13.2 °C; OFF	
Humidifier	inlet air Dew point <10.4 °C; ON	Dew point temp: 10.4 °C
	inlet air Dew point $\geq$ 10.4 °C; OFF	

conditions of a temperature of 13.2 °C and a humidity ratio of 0.00786 kg/kg, the humidification efficiency of WSS can be calculated using Eq. (3).

$$eff_{WSS} = \frac{\left(T_{H/C2,set} - 13.2°C\right)}{\left(T_{H/C2,set} - 11.62°C\right)} \tag{3}$$

3.2. Theoretical modelling for indirect cascade heat pump system

3.2.1. High-cycle heat pump

The performance of HCHP was confirmed by referring to previous research studies [9,25] that can predict the heat pump performance. Liu et al. studied a centrifugal heat pump using R-134a in a previous study. In Ref. [9], a performance prediction model was established under the conditions shown in Table 5, and Fig. 8 shows the refrigeration cycle of the heat pump.

The condenser load can be calculated as in Eq. (4), and the refrigerant temperatures of the evaporator and condenser were confirmed through Eqs. (5) and (6). Approach temperature implies the difference between the refrigerant temperature and the leaving water temperature of the evaporator and condenser.

$$Q_{cond,HCHP} = \dot{m}_{ref,total} \times (h_5 - h_6) \tag{4}$$

$$T_{ref,cond} = T_{HW,out} + T_{approach,HCHP} \tag{5}$$

$$T_{ref,evap} = T_{CW,out} - T_{approach,HCHP} \tag{6}$$

The intermediate refrigerant pressure and flow rate of the two-stage cycle can be calculated as follows [25]:

$$P_{med} = \sqrt{P_{cond} \times P_{evap}} \tag{7}$$

$$\dot{m}_{ref,evap} = \dot{m}_{ref,total} \times \left(1 - \frac{1 - \left(h_{exp,2,out} - h_{exp,1,in}\right)}{h_{med} - h_{exp,1,in}}\right) \tag{8}$$

$$\dot{m}_{ref,med} = \dot{m}_{ref,total} - \dot{m}_{ref,evap} \tag{9}$$

Compressor work of HCHP $W_{comp,HCHP}$ is the sum of the power consumption of one-stage and the two-stage compressors, and it considers the pressure loss of 1 %. The isentropic efficiency was considered as 85 %. Point 2′ on the pressure–enthalpy chart is compressed by the one-stage compressor when there is no pressure loss. When the pressure loss is reflected at point 2, the pressure at point 2′ can be found using Eq. (10), assuming an isentropic compression process. If the pressures at points 2′ and 5′ is known, the enthalpies at those points can be known, and the work of the one, two-stage compressors can be calculated by Eqs. (12) and (13). $W_{comp,HCHP}$ is the sum of $W_{1-stage,HCHP}$ and $W_{2-stage,HCHP}$, as depicted in Eq. (14). For the simulation, the following assumptions were applied: (1) The simulation was limited to steady-state analysis; (2) Compressor efficiency only considered isentropic efficiency; (3) Pressure loss and heat loss of other components, except the compressor, were neglected.

$$P_{2'} = P_1 + (P_2 - P_1) \times \frac{1}{1 - pressure\ loss} \tag{10}$$

$$P_{5'} = P_4 + (P_5 - P_4) \times \frac{1}{1 - pressure\ loss} \tag{11}$$

$$W_{1-stage,HCHP} = \dot{m}_{ref,evap} \times (h_{2'} - h_1) \tag{12}$$

$$W_{2-stage,HCHP} = \dot{m}_{ref,total} \times (h_{5'} - h_4) \tag{13}$$

$$W_{comp,HCHP} = \frac{W_{1-stage,HCHP} + W_{2-stage,HCHP}}{eff_{isentropic}} \tag{14}$$

Table 5
Parameters for high-cycle heat pump system simulation.

Parameter	Set point
Degree of subcooling and superheat	Subcooling: 2 °C, Superheat: 0.5 °C
Evaporator inlet and outlet temperature	Inlet: 30 °C, Outlet: 27.5 °C
Range of condenser outlet water temperature	55–85 °C
Condenser inlet and outlet water temperature difference	5 °C
Refrigerant approach temperature	1 °C
Isentropic efficiency of compressor	85 %
Pressure loss during compression	1 %
Total refrigerant flow rate	30 kg/s

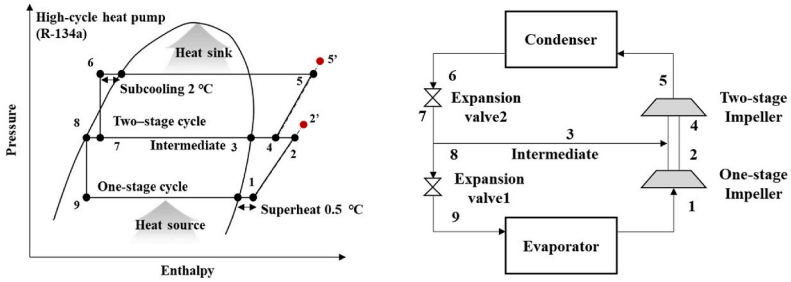

(a) Pressure-enthalpy diagram of high-cycle heat pump (b) Schematic of high-cycle heat pump

Fig. 8. Pressure–enthalpy diagram and schematic of high-cycle heat pump.

Table 6
Validation results of the heating coefficient of performance.

Condenser in, outlet water temperature range	Heating coefficient of performance		Error
	Liu et al.	Simulation results	
80–85	3.80	3.842	1.1 %
75–80	4.25	4.255	0.1 %
70–75	4.70	4.725	0.5 %
65–70	5.25	5.277	0.5 %
60–65	5.90	5.944	0.7 %
55–60	6.75	6.777	0.4 %
50–55	7.75	7.854	1.3 %

The heating COP was finally derived, as shown in Eq. (15), and the maximum error was within 2 % because of the comparison with the simulation results proposed by Liu et al., as shown in Table 6. The COP values were roughly confirmed in the COP change chart according to the HW temperature.

$$COP_{heat} = \frac{Q_{cond,HCHP}}{W_{comp,HCHP}} \tag{15}$$

Liu et al. had confirmed the COP until the condenser outlet water temperature reached 90 °C using simulation logic. However, the validation was performed only up to 70 °C; thus, further development of the logic is needed. Liu's simulation logic had the following problems: (1) Motor efficiency was not considered; (2) There was no change in compressor efficiency according to PR. In the experimental paper conducted by Liu et al., the motor remained insulated. This indicates that the motor was cooled by the refrigerant, and the condenser load increased. Therefore, the motor efficiency was assumed to be 95 %, and the heat loss was 5 % of the condenser load. The compressor work and condenser load of HCHP were modified as depicted in Eqs. (16) and (17). The isentropic efficiency according to the PR was demonstrated, as shown in Table 7 [11].

$$W_{comp,HCHP} = \frac{W_{1-stage,HCHP} + W_{2-stage,HCHP}}{eff_{motor} \times eff_{isentropic}} \tag{16}$$

$$Q_{cond,HCHP} = \dot{m}_{ref,total} \times (h_5 - h_6) + W_{comp,HCHP} \times 0.05 \tag{17}$$

In conclusion, the improved heating and cooling COPs were calculated in Eqs. (15) and (18), and the evaporator load using the cooling cop was confirmed in Eq. (19).

$$COP_{cool} = COP_{heat} - 1 \tag{18}$$

$$Q_{evap} = COP_{cool} \times W_{comp,HCHP} \tag{19}$$

Table 7
The isentropic efficiency according to the pressure ratio of compressor.

Pressure ratio	Isentropic efficiency
1.3	79 %
1.6	80 %
1.9	79 %
2.2	78 %
2.5	76 %

In this study, 86 °C HW1 was supplied from HCHP and used for the air heating of OAC, and the HW1 temperature returned to the condenser varied. At this time, the temperature of CW1 supplied to the HCHP was assumed to be five cases as shown in Fig. 5. As the temperature of the LCHP leaving CW1 increased, the PR of HCHP decreased, and the COP of HCHP improved. However, this increase in temperature reduced the performance of LCHP. Therefore, it was necessary to confirm how the temperature of the evaporator leaving CW1 affects the overall performance of CCHPS.

3.2.2. Low-cycle heat pump: centrifugal chiller

LCHP is assumed to be a centrifugal chiller using R-123 installed at Samsung Electronics. Of course, R-123 refrigerant is classified as non-ecological refrigerant due to high Global warming potential. However, in this study, the decision was made to consist a CAHPS using the originally installed R-123 chiller, and therefore, the option of using a chiller with a new refrigerant was not considered. The temperature of the CHW produced by the chiller is fixed at 12 °C. However, the temperature of the CW changes seasonally or is set to a high temperature for waste heat recovery. Therefore, a simulation logic that can predict the COP of a chiller based on the CW temperature is needed.

In Section 3.2.1, it is assumed that the CW1 flowing into the evaporator of HCHP is five cases. At this time, the lower the temperature of the CW1, the lower the PR of the LCHP, resulting in better performance for the LCHP. The reason why the maximum temperature of CW1 that can exit the chiller condenser is 39 °C, is as follows. Various equipment interlocks are set in the chiller to protect the equipment. In the condenser, the chiller is set to be off when the refrigerant pressure is 204.3 kPa to prevent excessive refrigerant pressure rise. Reflecting the safety factor of 20 % based on the refrigerant pressure of 204.3 kPa, it becomes 163.44 kPa, and the temperature of the refrigerant at this time is about 41.7 °C. In this study, the refrigerant approach temperature of the LCHP was assumed as 2 °C, and accordingly, when the condenser refrigerant temperature is 41 °C, the temperature of the CW1 that can be discharged from the condenser is 39 °C.

3.2.2.1. Theoretical performance calculation logic. For performance prediction, a theoretical simulation model was proposed by using operating data of the chiller operated at the Samsung Electronics. The pressure–enthalpy diagram for the chiller is depicted in Fig. 9.

Assumably, the inlet and outlet temperature difference of CW and CHW flowing through the condenser and evaporator was 5 °C. Therefore, CHW of 17 °C flows into the evaporator and is cooled to 12 °C, and CW enters the condenser and is heated by 5 °C. The variables used in the theoretical simulation logic can be checked in Table 8.

The temperature of the refrigerant in the condenser and evaporator were found using Eqs. (5) and (6). Evaporator load was expressed in Eq. (20) as the CHW cooling load. In this study, specific heat at constant pressure of water is assumed to be 4.19 kJ/kg°C.

$$Q_{evap,LCHP} = \dot{m}_{CHW} \times c_{p,water} \times \left(T_{CHW,in} - T_{CHW,out}\right) = \dot{m}_{ref,evap} \times (h_1 - h_9) \tag{20}$$

The flow rate of the refrigerant flowing through the evaporator can be determine through Eq. (20), and the flow rate of the refrigerant flowing through the condenser could be known using Eq. (8). LCHP compressor work could be known as the sum of one-stage and two-stage compressor works. Refrigerant pressure of points 2, 2′, and 5’ on Fig. 9(a) are calculated by using Eqs. (7), (10) and (11). Assuming an isentropic compression, the enthalpy of points 2′ and 5′ can be known, and the work of the one, two-stage compressors can be calculated using Eqs. (21) and (22). Finally, LCHP compressor work was calculated using Eq. (23).

$$W_{1-stage,LCHP} = \dot{m}_{ref,evap} \times (h_{2'} - h_1) \tag{21}$$

$$W_{2-stage,LCHP} = \dot{m}_{ref,total} \times (h_{5'} - h_4) \tag{22}$$

$$W_{comp,LCHP} = \frac{W_{1-stage,LCHP} + W_{2-stage,LCHP}}{eff_{motor} \times eff_{isentropic}} \tag{23}$$

Cooling COP and heating COP were confirmed using Eqs. (24) and (25). Condenser load of LCHP is calculated using Eq. (26) using heating COP.

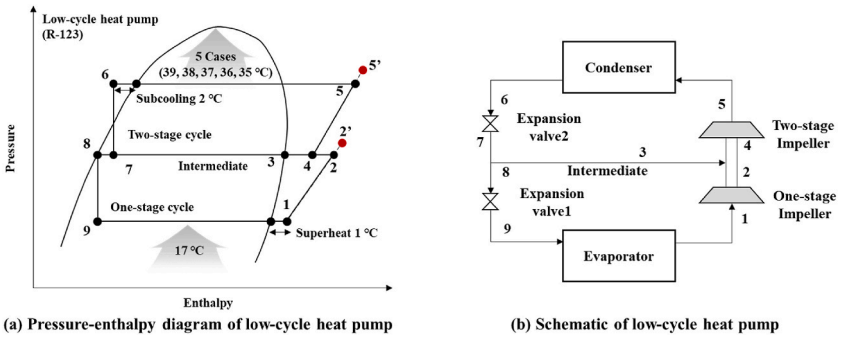

(a) Pressure-enthalpy diagram of low-cycle heat pump (b) Schematic of low-cycle heat pump

Fig. 9. Pressure–enthalpy diagram and schematic of the low-cycle heat pump.

Table 8
Parameters for low-cycle heat pump system simulation.

Parameter	Set point
Subcooling and superheat	Subcooling: 2 °C, Superheat: 1 °C
Evaporator inlet, outlet temperature	Inlet: 17 °C, Outlet: 12 °C
Range of condenser outlet water temperature	35–39 °C
Condenser inlet, outlet water temperature difference	5 °C
Refrigerant approach temperature	2 °C
Pressure loss during compression	1 %

$$COP_{cool} = \frac{Q_{evap,LCHP}}{W_{comp,LCHP}} \tag{24}$$

$$COP_{heat} = COP_{cool} + 1 \tag{25}$$

$$Q_{cond,LCHP} = COP_{heat} \times W_{comp,LCHP} \tag{26}$$

In this study, as mentioned above, the temperature of CHW supplied by the evaporator is fixed at 12 °C, and the temperature of CW can be changed. When the CW temperature varies, the PR of compressor changes, and the isentropic efficiency changes in response to the PR change. The isentropic efficiency according to PR was confirmed in the next section using actual chiller operation data.

3.2.2.2. Validation of isentropic efficiency according to compression ratio of chiller. For isentropic efficiency calculation, the chiller installed in Samsung Electronics was referred to, and the specifications of chiller are shown in Table 9.

Among the total 8760 h data, data were selected based on the following criteria: (1) The refrigerant approach temperature of the condenser and evaporator is less than 2 °C; (2) The flow measurement range of CHW is 600–800 m^3/hr. As a result of data reduction, only 1520 h of operation data was confirmed. Detailed operating data could be found in Appendix 1.

The compressor power consumption and cooling COP were confirmed using the operation data. Compressor power consumption could be found in Appendix 1, and cooling load was calculated via Eq. (27).

$$Q_{evap,data} = \dot{m}_{CHW} \times c_{p,water} \times \left(T_{CHW,in} - T_{CHW,out}\right) \tag{27}$$

The flow rate of CHW was confirmed using the differential pressure of CHW. As shown in Table 10, the chiller manufacturer provides the flow rate of CHW corresponding to the three differential pressure values, and the correlation between differential pressure and flow rate was confirmed through regression analysis using the three values.

Eq. (28) represents the correlation between the differential pressure and flow rate of cold water, where R^2 is 1.

$$V_{CHW} = \left(-247.09 \times DP^2 + 1,124 \times DP + 148.9\right) \times \rho_{water} \div 3,600\ sec \tag{28}$$

Next, all operation data were substituted into the parameters of the theoretical simulation logic in section 3.2.2.1. Subsequently, the isentropic efficiency was confirmed when the compressor work calculated through theoretical simulation logic the compressor work calculated with operating data were the same. The calculated isentropic efficiency is shown in Fig. 10, and isentropic efficiency varied with the PR changes. Among the heat pump research cases, Jankovic et al. also used isentropic efficiency calculation logic according to PR [26]. Therefore, PR was calculated using the refrigerant pressure of the condenser and evaporator of the operation data used in this study, and then the correlation between the calculated isentropic efficiency and PR was analyzed by regression, as shown in Fig. 10.

As a result of regression analysis, R^2 was confirmed as 0.9898, and isentropic efficiency could be calculated differently according to PR using Eq. (29).

$$eff_{isentropic} = -0.1423 \times PR^3 + 0.8373 \times PR^2 + 0.965 \tag{29}$$

To verify the consistency of the isentropic efficiency, Eq. (29) was used as the efficiency in Eq. (23) in Section 3.2.2.1, and the result of calculating $W_{comp,LCHP}$ using operation data is shown in Fig. 11. When compared with the power calculated using operation data, the error within ±10 % was satisfied under the condition of operation data of 1520 h.

Finally, the isentropic efficiency formula using PR as a variable was substituted into Eq. (23) to calculate the LCHP compressor work.

Table 9
Specifications of the centrifugal chiller installed in Samsung Electronics.

Specification	Value
Refrigerant	R 123
Capacity	1700 usRT
Flow rate of cooling water	1193.78 m^3/hr
Flow rate of chilled water	1027.73 m^3/hr
Voltage	6600 V

Table 10
Chilled water flow rate information according to the differential pressure.

Differential pressure of chilled water	Flow rate of chilled water
1.76 kgf/cm^2	1361.30 m^3/hr
1.00 kgf/cm^2	1027.73 m^3/hr
0.03 kgf/cm^2	185.64 m^3/hr

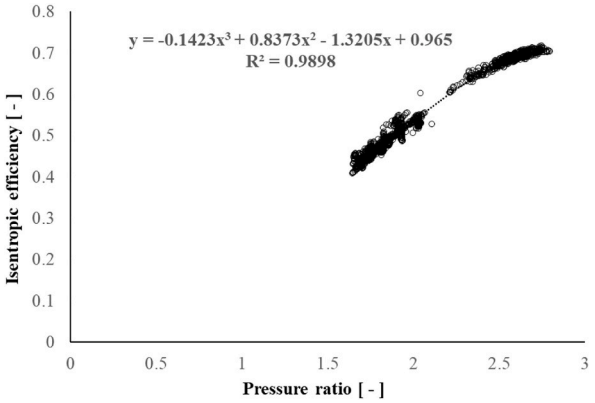

Fig. 10. Correlation between the pressure ratio and isentropic efficiency.

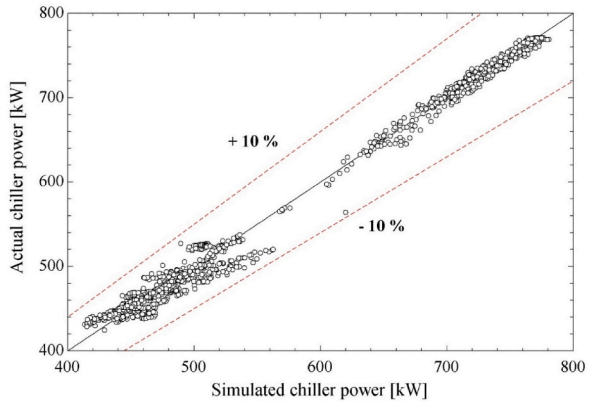

Fig. 11. Validation of theoretical calculation for low-cycle heat pump compressor work.

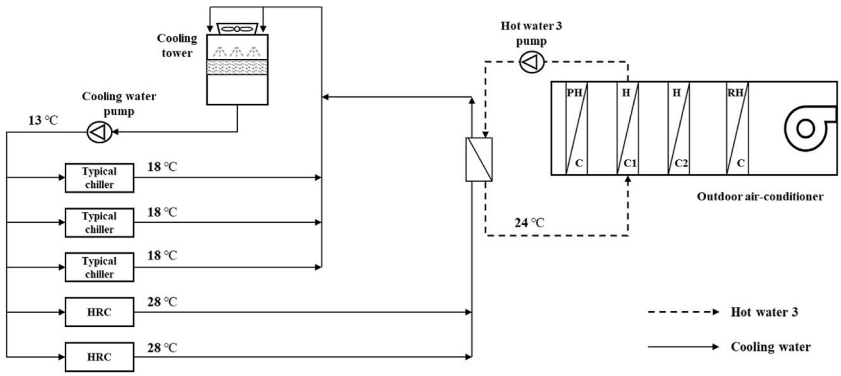

Fig. 12. Difference between the cooling water circulation system of the typical chiller and heat recovery chiller.

3.2.3. Heat recovery chiller

In a typical chiller, CHW at 17 °C is cooled to 12 °C in an evaporator. Simultaneously, waste heat is transferred to the CW in a condenser, and finally, the heat is radiated to the outdoor air at a cooling tower. However, the HRC uses the CW2 from the condenser as a heat source instead of directly transferring it to the cooling tower. In the air-conditioning system at Samsung Electronics, waste heat generated from the HRC is reused as a heat source for H/C1. Therefore, even when CCHPS is applied as a heat source of OAC, the heat source of H/C1 uses CW, which is the waste heat from HRC. The HRC is the same equipment as the chiller; however, it maintains a higher CW temperature leaving the condenser. As shown in Fig. 12, HRC receives CW from the cooling tower, but unlike the chiller, the CW2 leaving the condenser transfers waste heat to the HW3 that circulates H/C1.

In addition, to satisfy the design condition of 24 °C of HW3 circulating through H/C1, in this study, the CW2 temperature leaving the HRC condenser was maintained at a minimum of 28 °C. When the condenser entering temperature of CW of HRC is 23 °C or higher, it is assumed that the temperature rises by 5 °C and exits the condenser at 28 °C or higher. When the temperature of condenser entering CW is below 23 °C, the CW flow rate flowing through the condenser should be reduced to maintain the outlet CW2 temperature high.

HRC and LCHP are essentially the same facility; thus, the performance prediction of HRC was calculated in the same process as LCHP by referring to section 3.2.2.

3.2.4. Heat exchanger and pump

The HW1 supplied by the HCHP heat exchanges with antifreeze solution circulating in PH/C, and HW2 circulating in H/C2 and RH/C through plate heat exchangers A and B, respectively. The coil inlet temperature of the antifreeze solution and HW2 is 80 °C, and the flow rate and coil outlet temperature according to outdoor air conditions can be known through TRNSYS. At this time, the heat-exchanger efficiency is assumed as 75 %, and the flow rate and temperature of HW1 to be supplied from the HCHP after heat exchange can be calculated using the effective method. In the heat exchangers A and B, the cold side contains the antifreeze solution and HW2, respectively, and the hot side contains HW1. Q_{real} is the actual heat transfer rate, and Q_{max} is the theoretical maximum heat transfer rate. The heat exchange process was calculated using the formula below:

$$Q_{real} = \varepsilon \times Q_{max} = \varepsilon \times C_{min} \times \left(T_{h,in} - T_{c,in}\right) \tag{30}$$

$$C_{min} = Minimum\ value\ of C_c\left(c_{p,c} \times \dot{m}_c\right)\ and C_h\left(c_{p,h} \times \dot{m}_h\right) \tag{31}$$

$$Q_{real} = \dot{m}_h \times c_{p,h} \times \left(T_{h,in} - T_{h,out}\right) = \dot{m}_c \times c_{p,c} \times \left(T_{c,out} - T_{c,in}\right) \tag{32}$$

In this study, C_{min} can be confirmed by referring to Eq. (31), and it is assumed that C_h, the heat capacity rate of the HW1 supplied from the heat pump, becomes C_{min}. Therefore, for C_h to have a value below C_c throughout the year, the minimum HW1 temperature supplied by the heat pump is calculated as 86 °C. In the same way as above, it was possible to assume that the lowest temperature of CW2 supplied from HRC was 28 °C, and the temperature of CW2 that heat exchanged with HW3 circulating H/C1 could be known.

If the flow rate of the fluid circulating through HCHP, LCHP, and HRC is known, the power consumption of the pump can be calculated. The head of the pump was determined, as shown in Table 11, by referring to the chiller system installed in Samsung Electronics.

Pump efficiency was assumed as 80 %, and the power consumption of the pump can be calculated using Eq. (33).

$$W_{pump} = \frac{\dot{m}_{fluid} \times head[m]}{102 \times \varepsilon_{pump}} \tag{33}$$

3.3. Theoretical modelling for steam boiler system

The OAC installed in Samsung Electronics uses the steam produced by the boiler. In this study, a steam boiler system was selected as a reference system to compare the energy consumption. In the OAC system using a boiler, the antifreeze solution and HW2 use the steam as a heat source.

3.3.1. Fuel consumption

Boiler burns natural gas to produce steam; thus, it is important to calculate natural gas consumption. Boiler system can be represented as Fig. 6.

The boiler is the water-tubbed-type and consists of a fan, feed-water pump, main body, and economizer. Feed water temperature and pump as well as fan specifications were assumed by referring to the actual boiler system, as shown in Table 12.

Efficiency of boiler was assumed as 95 %, and steam production per 1 Nm^3 of natural gas was calculated using the direct method [27] as follows:

Table 11
Pump heads according to the different types of water.

Equipment	HCHP, LCHP, HRC, Typical chiller		
Type of water	Hot water1	Cooling water1, 2	Chilled water
Head of pump (m)	45	30	45

Table 12
Specification of the boiler system.

Specification	Value
Boiler efficiency	95 %
Feed water temperature	85 °C
Steam evaporation	10 ton/hr
Steam pressure	686.5 kPa (=7 kg/cm^2)
Dryness	0.98
Pump efficiency	51.9 %
Fan efficiency	52.3 %
Feed water pump head	119 m
Static pressure of fan	380 mmAq (3.73 kPa)

$$eff_{boiler} = \frac{Heat\ output}{Heat\ input} = \frac{Heat\ output}{LHV_{natural\ gas}} \tag{34}$$

$$Heat\ output = S \times \left(h_{steam} - h_{feed\ water}\right) \tag{35}$$

$$h_{steam} = h_{saturated\ water} + dryness \times h_{latent,steam} \tag{36}$$

where $LHV_{natural\ gas}$ is the low heating value of natural gas: 9190 $kcal/Nm^3$ [29], and $h_{feed\ water}$ is the enthalpy of the feed water (=85 kcal/kg) at 85 °C, and S [kg/Nm^3] is the steam evaporation per 1 Nm^3 of fuel, and $h_{saturated\ water}$ is the enthalpy of saturated water (=171.21 kcal/kg) at a pressure of 686.5 kPa and $h_{latent,steam}$ is the latent heat enthalpy of steam (=489.73 kcal/kg) at a pressure of 686.5 kPa.

As a result of the calculation, the boiler can produce 15.42 kg of steam per 1 Nm^3 of natural gas, and the steam is used after being reduced to 196.1 kPa at the place of use. Steam uses latent heat for heat exchange; thus, it has a heat quantity of 2201.6 kJ/kg based on a pressure of 196.1 kPa [28]. The required amount of steam can be calculated using Eq. (37). After checking the amount of steam, the amount of natural gas used for combustion can be calculated through Eq. (38) using 15.42 kg/Nm^3 calculated in Eq. (35).

$$\dot{m}_{steam} = Q_{heatsink} \times 3,600[sec] \div 2,201.6[kJ/kg] \tag{37}$$

$$V_{natural\ gas} = \dot{m}_{steam} \div S \tag{38}$$

3.3.2. Fan and pump

For boiler combustion and steam production, it is important to supply air required for the combustion process and feed water required for steam production. Specification related to fan and pump can be found in Table 6. Feed water supply is assumed equal to steam evaporation, and power consumption of pump can be calculated through Eq. (33). The theoretical air volume required for combustion can be calculated by multiplying the theoretical air fuel ratio by the natural gas flow rate, and the theoretical air fuel ratio can be calculated through Eq. (39) [27]. Finally, the air flow rate and power consumption of the fan can be calculated using Eqs. (40) and (41).

$$Theoretical\ air\ fuel\ ratio = 2.68 \times 4.186[kJ/kcal \bullet kg] \times LHV_{natural\ gas} \div 10,000 \tag{39}$$

$$V_{combustion\ air} = Theoretical\ air\ fuel\ ratio \times V_{natural\ gas} \tag{40}$$

$$W_{fan,boiler} = \frac{V_{combustion\ air} \times Static\ pressure\ loss\ [kpa]}{3,600[sec] \times \varepsilon_{fan,static}} \tag{41}$$

3.4. Total energy consumption of heating equipment for outdoor air-conditioner

3.4.1. Energy consumption calculation logic

CCHPS uses 100 % electricity to produce HW1, and the boiler system mainly burns natural gas to produce steam. Therefore, a different approach is needed when estimating the total energy consumption of the two systems.

In CCHPS, LCHP has the advantage of producing CHW while supplying high-temperature CW1 to HCHP. Therefore, the power consumption of the typical chiller can be reduced, while CCHPS supplies HW1. However, based on the same CHW supply, the LCHP operates inefficiently and consumes more power than a typical chiller. This is because the LCHP has a higher condenser refrigerant pressure than a typical chiller to provide high-temperature CW. Similarly, HRC also produces CHW while supplying heat to H/C1 and operates less efficiently than a typical chiller when the condenser inlet CW temperature is below 23 °C. In conclusion, it is confirmed that the power of LCHP and HRC reflects only the additional power consumption caused by operating less efficiently than a typical chiller for the same CHW supply.

Therefore, the power consumed when the typical chiller produces as much as the CHW produced by LCHP and HRC must be reflected as power saving. At this time, the operation of the cooling tower and CW pump required for CW cooling in a typical chiller system is also unnecessary, and it must be reflected in the amount of power saving. The power consumption of typical chiller, cooling

tower, and CW pump is detailed in Section 3.4.3. The total energy consumption of the heating equipment for OAC with CCHPS and HRC can be calculated using Eqs. (42) and (43).

$$\sum W_{OAC,CCHPS} = \sum W_{HCHP} + \sum W_{LCHP} + \sum W_{pump,CCHPS} + \sum W_{HRC} + \sum W_{pump,HRC} + \sum W_{cooling\ tower,HRC} - \sum W_{saving} \tag{42}$$

$$\sum W_{saving} = \sum W_{chiller} + \sum W_{cooling\ tower} + \sum W_{CW\ pump} + \sum W_{CHW\ pump} \tag{43}$$

The heating system COP can be calculated using Eq. (44), and it can be seen as a heating COP considering the sum of facility power used for heating. Heating system COP can be calculated separately from CCHPS and HRC, and various cases can be considered depending on whether power saving is reflected or not.

$$COP_{heat,system} = \frac{Q_{cond,HCHP} + Q_{cond,HRC}}{\sum W_{OAC,CCHPS}} \tag{44}$$

The total energy of the heating equipment for the OAC with the boiler needs to consider the amount of natural gas used for combustion and the power energy required for fan and pump operation. There is no side effect such as CHW production by boiler operation; thus, there is no need to consider power saving. However, HRC supplying heat to H/C1 does not change; hence, power saving is considered as Eq. (43). The total energy of the heating facility for the OAC with the boiler applied can be expressed as Eqs. (45)–(47).

$$\sum W_{OAC,Boiler} = \sum W_{electricity,Boiler} + \sum Q_{natural\ gas,Boiler} \tag{45}$$

$$\sum W_{electricity,Boiler} = \sum W_{fan,Boiler} + \sum W_{pump,Boiler} + \sum W_{HRC} + \sum W_{pump,HRC} + \sum W_{cooling\ tower,HRC} - \sum W_{saving} \tag{46}$$

$$\sum Q_{natural\ gas,Boiler} = \sum V_{natural\ gas} \times LHV_{natural\ gas} \div 860[kcal/kW] \tag{47}$$

OAC with CCHPS is supplied with heat from the heating equipment using 100 % electrical energy. However, the boiler uses both electric and gas energies. Therefore, it is necessary to convert these to the primary energy for equal comparison. Finally, the primary energy consumed by the heating equipment of the OAC system with CCHPS and boiler can be expressed using Eqs. (48) and (49), respectively.

$$\sum E_{OAC,CCHPS} = \sum W_{OAC,CCHPS} \times 2.75 \tag{48}$$

$$\sum E_{OAC,Boiler} = \sum W_{electricity} \times 2.75 + \sum Q_{natural\ gas} \times 1.1 \tag{49}$$

where 2.75 is the primary energy conversion factor for electricity, and 1.1 is the primary energy conversion factor for natural gas in South Korea [30].

3.4.2. Carbon dioxide emission calculation logic

Heating equipment applied to OAC generates heat by using electricity or burning natural gas. At this time, carbon dioxide is emitted by the electricity and natural gas used. In this study, the amount of carbon dioxide emissions was calculated using the carbon emission factor of South Korea in the following manner [31]:

$$\sum CO_2 = \sum W_{electricity} \times 0.4747 \mathrm{kg}CO_2 \Big/ kWh + \sum V_{natural\ gas} \times 2.41 \mathrm{kg}CO_2 \Big/ m^3 \tag{50}$$

where 0.4747 is the carbon dioxide emission factor for electricity, and 2.41 is the emission factor for natural gas of South Korea. In this study, only carbon dioxide emissions from electricity and natural gas usage were taken into account, while emissions from refrigerant leaks and gas leaks were not included.

3.4.3. Typical chiller system

LCHP and HRC consume more electricity than typical chillers because they need to supply high-temperature CW. Supplying high-temperature CW means that the refrigerant temperature of condenser rise, resulting in an increase in PR. Therefore, it is necessary to calculate the operating power of a typical chiller based on the production of the same CHW to determine how much additional power is consumed due to inefficient operation of the LCHP and HRC. The temperatures of inlet and outlet CHWs of a typical chiller are 17 °C and 12 °C, respectively, and the temperature difference between the inlet and outlet CW flowing through the condenser is 5 °C. However, if the temperature of inlet CW is below 13 °C, the temperature of outlet CW should be at least 18 °C. The oil circulation

Table 13
Temperature of the water leaving condenser.

	Classification of chillers according to the purpose of use		
	Low-cycle heat pump (Cooling water1)	Heat recovery chiller (Cooling water2)	Typical chiller (Cooling water)
Temperature [°C]	35, 36, 37, 38, 39 (5 Cases)	28~39	18~39

system of the chiller installed in Samsung Electronics can operate stably when the difference in refrigerant pressure between the condenser and the evaporator exceeds 20.7 kPa. Therefore, considering the safety factor of 20 %, the minimum refrigerant pressure difference between the condenser and the evaporator should be about 25 kPa. As the approach temperature is assumed as 2 °C in Section 3.2.2, when producing 12 °C CHW, the refrigerant temperature and pressure in the evaporator are 10 °C and are 50.65 kPa, respectively. At this time, when the condenser refrigerant temperature is 20 °C, the refrigerant pressure becomes 75.71 kPa, and it is possible to secure a differential pressure of 25 kPa. When the approach temperature is 2 °C, the condenser refrigerant temperature becomes 20 °C, and the temperature of condenser leaving CW is 18 °C. In conclusion, when the condenser inlet CW is lower than 13 °C, the outlet CW temperature is assumed as 18 °C unconditionally. LCHP, HRC, and a typical chiller are the same equipment in terms of producing CHW; however, in this study, they are classified differently according to the temperature of CW leaving condenser, as shown in Table 13. The COP of a typical chiller can be calculated by referring to Section 3.2.2.

Knowing the power consumption of a typical chiller, LCHP, and HRC based on producing the same CHW, it is possible to calculate the additional power consumption resulting from inefficient operation of the LCHP and HRC. In addition, it is necessary to check the operating power of the cooling tower, CW pump, and CHW pump used by the typical chiller system. This is because when LCHP and HRC produce CHW, the operating load of the typical chiller is reduced, and the operating load of the cooling tower, CW pump, and CHW pump is also reduced. The specifications of the cooling tower installed in Samsung Electronics are shown in Table 14 [1], and the power consumption of the CW pump, CHW pump, and cooling tower fan can be calculated using Eqs. (33), (51) and (52). The head values of the CW pump and CHW pump are presented in Table 11.

$$\dot{m}_{air,cooling\ tower} = \dot{m}_{CW} \div 1.27 \tag{51}$$

$$W_{fan,Cooling\ tower} = \frac{\dot{m}_{air,cooling\ tower} \times Static\ pressure\ loss[kpa]}{\rho_{air} \times \varepsilon_{fan,static}} \tag{52}$$

4. Results and discussion

4.1. Annual heating load of outdoor air-conditioner

The annual heating load of an OAC with a 2000 m^3/min fan was calculated through TRNSYS. As a result of checking the annual air-heating load for each heating coil, RH/C load was the least, followed by PH/C, H/C2, and H/C1 sequentially. RH/C has the least load among heating coils and is mainly used in summer. PH/C is used to raise the air temperature below 0 °C to prevent OAC coil from freezing. Since it is used only during the winter season, it belongs to the low-load side among OAC heating coils. Lastly, the loads of H/C2 and H/C1 are the highest, and as the outdoor temperature/humidity increases, the load of H/C2 decreases compared to that of H/C1. The heating load of each coil is shown in Fig. 13.

The sum of the heating loads using HW2 and antifreeze solution is 45.8 % of the annual total heating load, and the H/C1 load using HW3 is 54.2 % of the total heating load. Currently, the OAC uses steam to heat HW2, and HW3 uses CW2 from HRC as a heat source. Therefore, even when CCHPS is applied to OAC, it is reasonable to use CW2 as a heat source for HW3 heating. The return temperatures of the antifreeze solution, HW2 and HW3 circulating through each coil can be seen in Fig. 14.

In this study, cleanroom heating energy with an OAC of 20,000 m^3/min was analyzed, and the total heating load was 35,625,222 kWh. Among the total loads, the heating load of H/C1 is 19,318,824 kWh, and the heating load of the rest of the heating coil is 16,306,398 kWh.

4.2. Annual energy consumption of the cascade heat pump system and heat recovery chiller

4.2.1. Energy performance of cascade heat pump system and heat recovery chiller

The COP of HCHP and LCHP depends on the CW1 temperature from the LCHP condenser. Fig. 15(a) shows that the COP of LCHP decreases with higher CW1 temperature, while the COP of HCHP increases. Using the heat-pump COP, the annual condenser and evaporator loads of each heat pump can be calculated, as shown in Fig. 15(b). The condenser load of the HCHP heat pump is determined by the heating load of the OAC and remains constant regardless of the CW1 temperature. Based on Fig. 15(b), the evaporator load of the HCHP decreases with the decreasing CW1 temperature, while the evaporator load of LCHP increases until CW1 temperature reaches 37 °C and then starts decreasing from 36 °C.

In other words, the optimal CW1 temperature for producing the maximum CHW at 12 °C while supplying 86 °C HW1 to the OAC is 37 °C. These results can be explained using the COP of HCHP and LCHP. The evaporator load of LCHP, as described by Eq. (57), is influenced by the ratio of the COP of HCHP and LCHP.

$$COP_{ratio} = \frac{COP_{cool}}{COP_{heat}} \tag{53}$$

$$W_{comp,HCHP} = \frac{Q_{cond,HCHP}}{COP_{heat,HCHP}} \tag{54}$$

Table 14
Specifications of the cooling tower.

Cooling tower		Liquid-to-gas ratio	1.27
		Static pressure loss	18.62 mmAq (0.18 kPa)
		Static pressure efficiency	47.75 %

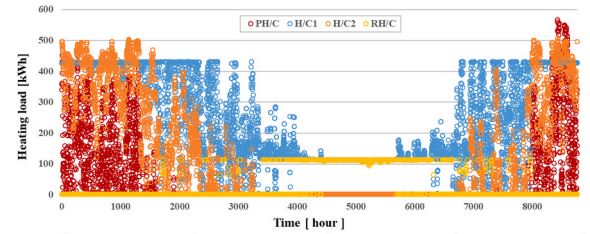

	Pre-heating coil	Heating coil 1	Heating coil 2	Re-heating coil
Annual load	305,504 kWh (8.6 %)	1,931,882 kWh (54.2 %)	1,060,763 kWh (29.8 %)	264,374 kWh (7.4 %)

Fig. 13. Annual heating loads of heating coils on outdoor air-conditioner.

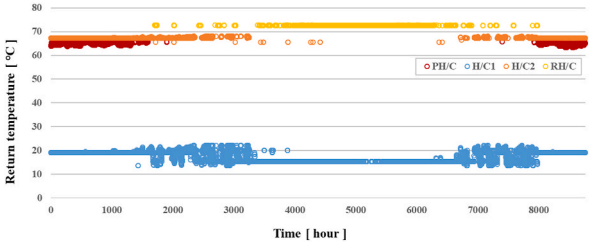

Fig. 14. Return temperature of antifreeze solution and hot water.

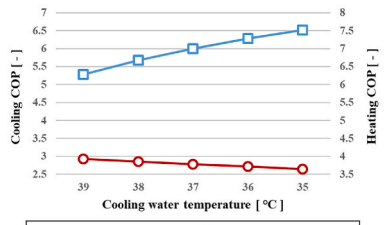

	High-cycle heat pump		Low-cycle heat pump	
	COP_{heat} [-]	COP_{cool} [-]	COP_{heat} [-]	COP_{cool} [-]
39 °C	3.93	2.93	6.288	5.288
38 °C	3.856	2.856	6.676	5.676
37 °C	3.785	2.785	7.006	6.006
36 °C	3.716	2.716	7.285	6.285
35 °C	3.649	2.649	7.519	6.519

(a) Coefficient of performance of heat pump

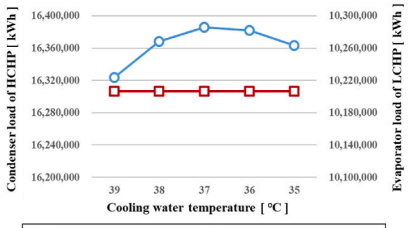

	High-cycle heat pump		Low-cycle heat pump	
	Condenser load [kWh]	Evaporator load [kWh]	Condenser load [kWh]	Evaporator load [kWh]
39 °C	16,306,398	12,157,187	12,157,187	10,223,793
38 °C	16,306,398	12,077,561	12,077,561	10,268,459
37 °C	16,306,398	11,998,235	11,998,235	10,285,669
36 °C	16,306,398	11,918,239	11,918,239	10,282,242
35 °C	16,306,398	11,837,668	11,837,668	10,263,300

(b) Verifying the annual evaporator load of LCHP in accordance with changes in cooling water temperature

Fig. 15. The impact of cooling water temperature on heat pump performance.

Table 15
Ratio of the coefficient of performance.

Cooling water1 temperature	$COP_{ratio,HCHP}$	$COP_{ratio,LCHP}$	$COP_{ratio,HCHP} \times COP_{ratio,LCHP}$
39 °C	0.746	0.841	0.6270
38 °C	0.741	0.850	0.6297
37 °C	0.736	0.857	0.6308
36 °C	0.731	0.863	0.6306
35 °C	0.726	0.867	0.6294

$$Q_{evap,HCHP} = COP_{cool,HCHP} \times W_{comp,HCHP} = COP_{ratio,HCHP} \times Q_{cond,HCHP} = Q_{cond,LCHP} \tag{55}$$

$$W_{comp,LCHP} = \frac{Q_{cond,LCHP}}{COP_{heat,LCHP}} = \frac{Q_{evap,HCHP}}{COP_{heat,LCHP}} = \frac{COP_{ratio,HCHP} \times Q_{cond,HCHP}}{COP_{heat,LCHP}} \tag{56}$$

$$Q_{evap,LCHP} = COP_{cool,LCHP} \times W_{comp,LCHP} = COP_{ratio,HCHP} \times COP_{ratio,LCHP} \times Q_{cond,HCHP} \tag{57}$$

Table 15 shows the ratio of the COP of HCHP and LCHP, and the value obtained by multiplying the ratio of the COP of HCHP and LCHP is the highest at 37 °C. Therefore, the largest LCHP evaporator load can be obtained when the CW1 temperature is 37 °C.

In addition, because of examining the power consumption of CCHPS according to the CW1 temperature, as shown in Fig. 16, the power consumption of CCHPS is the lowest when the CW1 temperature is 37 °C.

The power consumption of CCHPS is influenced by the compressor work of LCHP and HCHP, which can be analyzed using COP, as described in Eqs. (54) and (56). The compressor work of HCHP increases with the decreasing CW1 temperature due to the higher reciprocal value of the heating COP. Conversely, the compressor work of LCHP decreases as the CW1 temperature decreases because the value obtained by multiplying the ratio of COP of HCHP and the reciprocal of the heating COP of LCHP decreases. Refer to Table 16 for the COP values used to calculate the compressor work.

As the CW1 temperature decreases, the reduction rate of the LCHP compressor work is higher than the increase rate of the HCHP compressor work until 37 °C, and the opposite trend occurs from 36 °C. Therefore, the lowest sum of compressor work for the LCHP and HCHP is achieved when the CW1 temperature is set at 37 °C. Although there was a change in pump power consumption, it had a negligible impact due to its significantly lower proportion compared to the compressor. The annual COP of HRC is shown in Fig. 17. The HW3 circulating through H/C1 is maintained at 24 °C by exchanging heat with outlet CW2, which is at least 28 °C from the HCR condenser. The temperature of the inlet CW from the cooling tower and the outlet CW2 from the HCR condenser can be observed throughout the year in Fig. 17. Consequently, the annual condenser load is 35,367,265 kW, and the evaporator load is 31,164,273 kW. The annual power consumption of HRC can be classified by facility, as shown in Fig. 16, and the total power consumption is 5,425,160 kWh.

Consequently, at a CW1 temperature of 37 °C, the CCHPS power consumption reached its lowest point at 6,659,417 kWh, resulting in a system COP of 2.45 for handling the heating load of PH/C, H/C2, and RH/C. The HRC system achieved a COP of 3.56 for handling the heating load of H/C1. The total system COP of CCHPS and HRC combined was measured at 2.95.

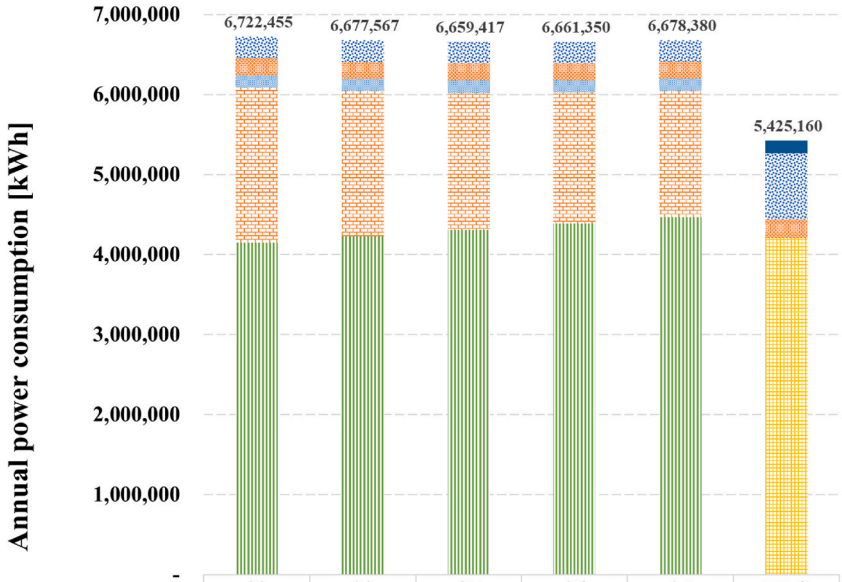

	39	38	37	36	35	HRC
Cooling Tower	0	0	0	0	0	163,000
CHW pump	269,123	270,298	270,752	270,661	270,163	820,343
CW Pump	213,344	211,947	210,554	209,151	207,737	238,824
HW1 Pump	157,383	157,383	157,383	157,383	157,383	0
HRC Compressor	0	0	0	0	0	4,202,993
LCHP Compressor	1,933,395	1,809,101	1,712,566	1,635,997	1,574,367	0
HCHP Compressor	4,149,211	4,228,838	4,308,163	4,388,159	4,468,731	0
Total	6,722,455	6,677,567	6,659,417	6,661,350	6,678,380	5,425,160

Fig. 16. Cascade heat pump system power consumption according to cooling water1 temperature and heat recovery chiller power consumption.

Table 16
Coefficient of performance values for compressor work calculation.

Cooling water1 temperature	$1/COP_{heat,HCHP}$	$COP_{ratio,HCHP} \times (1/COP_{heat,LCHP})$
39 °C	0.254	0.119
38 °C	0.259	0.111
37 °C	0.264	0.105
36 °C	0.269	0.100
35 °C	0.274	0.097

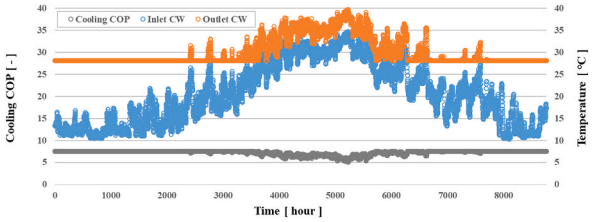

Fig. 17. The coefficient of performance and cooling water2 temperature of heat recovery chiller.

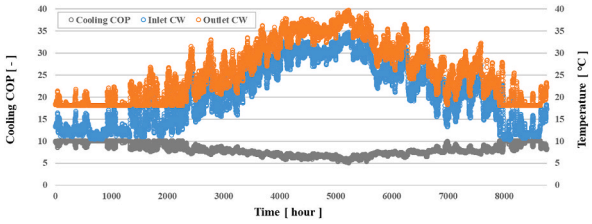

Fig. 18. The coefficient of performance and cooling water temperature of a typical chiller.

4.2.2. Total energy consumption of cascade heat pump system and heat recovery chiller

As CCHPS and HRC supply HW1 and CW2 to OAC and simultaneously produce CHW for FAB, it is possible to reduce CHW production of typical chillers. Since the reduced operation of a typical chiller leads to power saving, it is necessary to check the amount of power that can be saved when the typical chiller does not produce as much as the amount of CHW produced by CCHPS and HCR. The CHW production of CCHPS and HRC is equal to the evaporator load of LCHP and HRC. The year-round COP and CW temperature of a

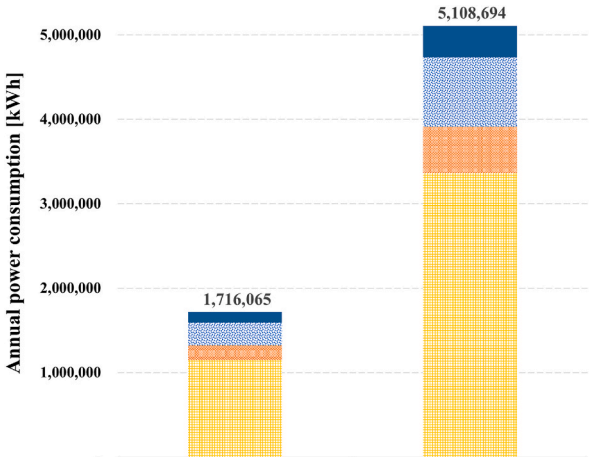

	Typical chiller (LCHP CHW)	Typical chiller (HRC CHW)
Cooling Tower	121,502	374,477
CHW pump	270,752	820,343
CW Pump	178,022	548,673
Compressor	1,145,790	3,365,202
Total	1,716,065	5,108,694

Fig. 19. The power savings of a typical chiller system.

Table 17
Heating system coefficient of performance comparison according to the cascade heat pump system combination.

Power	CCHPS	CCHPS-Saving	CCHPS + HRC	CCHPS + HRC-Saving
Heating system COP [-]	2.45 (100 %)	3.30 (135 %)	2.95 (100 %)	6.77 (230 %)
Consumption [MWh]	6659	6659	12,085	12,085
Saving [MWh]		1716		6825
Total [MWh]	6659 (100 %)	4943 (74 %)	12,085 (100 %)	5260 (44 %)

typical chiller are shown in Fig. 18, and the power of the general chiller system reduced due to CHW produced from LCHP and HRC are shown in Fig. 19.

The annual electricity consumed by CCHPS and HRC is 12,084,577 kWh; however, the amount of electricity saved by a typical chiller is 6,824,759 kWh, which is confirmed as a significant amount. The heating system COP before and after reflecting the power saved by CHW production is confirmed, as shown in Table 17.

When looking at CCHPS alone, there is a 26 % difference in energy consumption before and after the power saving is reflected, and the heating system COP reflecting saving appears to increase by 35 %. When checking heating system COP in OAC unit with CCHPS, the increase rate was larger, and when power saving was reflected, it was found to increase by 130 %. This is because the total power consumption of HRC was 5,425,160 kWh, while the power saving reached 5,108,694 kWh; thus, the total power consumption was only 316,466 kWh.

4.3. Comparison of energy usage between boiler system and cascade heat pump system

A boiler with a thermal efficiency of 95 % can produce 15.42 kg of steam per 1 m^3 of natural gas. Throughout the year, the OAC utilizes 26,664 tons of steam for air heating at a rate of 20,000 m^3/min. This corresponds to a natural gas consumption of 1,729,170 m^3. Additionally, the combustion air supply fan consumes 35,250 kWh of electricity, and the feed water pump consumes 16,649 kWh of electricity.

Even when a boiler system is applied as the heating equipment to OAC, H/C1 uses 28 °C CW2 from HRC as a heat source; hence, the power consumption of HRC system must be reflected in the energy consumed for annual OAC air heating. Therefore, the total energy consumed for air heating by OAC, which uses a boiler as the heating equipment, is the sum of 1,729,170 m^3 of natural gas and 5,477,059 kWh of electricity. When accounting for the power savings generated by the CHW produced by HRC, the total energy consumption becomes 1,729,170 m^3 of natural gas and 368,365 kWh of electricity.

To determine the suitability of CCHPS compared to existing boiler systems, a comparison of primary energy consumption and carbon dioxide emissions is necessary, as these systems employ different utilities. The results indicate that in all cases, the combination of heating equipment with CCHPS offers more advantages compared to the combination of heating equipment with a boiler. The primary energy comparison is shown in Table 18, with the primary energy consumption by CCHPS based on the CW1 temperature from the LCHP condenser at 37 °C.

When comparing only the energy consumed by the CCHPS and the boiler system, CCHPS consumes 11 % less energy. In addition, when considering CHW produced by CCHPS as an energy saving factor, it consumes 34 % less energy. To compare the total energy consumption of the heating equipment applied to OAC, (1) CCHPS and HRC, and (2) boiler and HRC energy consumption were compared. When comparing before and after reflecting the CHW produced from CCHPS and HRC as a saving factor, differences of 6 % and 32 % occurred, respectively. As a result of the above, the heating system that uses the heat source of the heat pump for cooling can have a great effect. A greater effect in terms of carbon dioxide emissions was also observed in the comparison, with results depicted in Table 19.

As with primary energy consumption, carbon dioxide emissions exhibited the same trend. It is advantageous to use CCHPS as a heating equipment option, whether or not the power-saving capabilities of a typical chiller system are considered. When comparing CCHPS with the boiler alone, a carbon emission reduction effect of 25 % was observed before considering power savings and 44 % after accounting for power savings. In addition, CCHPS and HRC emit 15 % less carbon emissions than boilers and HRC, and when power saving is reflected, a 42 % carbon emission reduction effect occurs.

In conclusion, when comparing CCHPS and boiler alone, CCHPS is advantageous. In addition, unlike general building heating, a

Table 18
Comparison of primary energy consumption between the cascade heat pump system and the boiler system.

Primary energy	Comparison of CCHPS and Boiler			Comparison of energy consumption for heating of OAC with CCHPS and OAC with boiler			
	CCHPS	CCHPS-Saving	Boiler	CCHPS + HRC	Boiler + HRC	CCHPS + HRC-Saving	Boiler + HRC-Saving
Consumption [MWh]	18,313	18,313	20,469	33,233	35,388	33,233	35,388
Saving [MWh]		4719				18,768	14,049
Total [MWh]	18,313 (89 %)	13,594 (66 %)	20,469 (100 %)	33,233 (94 %)	35,388 (100 %)	14,465 (68 %)	21,339 (100 %)

Table 19
Comparison of carbon dioxide emissions between the cascade heat pump system and the boiler system.

Carbon dioxide emissions	Comparison of CCHPS and Boiler			Comparison of energy consumption for heating of OAC with CCHPS and OAC with boiler			
	CCHPS	CCHPS-Saving	Boiler	CCHPS + HRC	Boiler + HRC	CCHPS + HRC-Saving	Boiler + HRC-Saving
Emissions [ton]	3162	3162	4192	5737	6767	5737	6767
Saving [ton]		815				3240	2425
Total [ton]	3162 (75 %)	2347 (56 %)	4192 (100 %)	5737 (85 %)	6767 (100 %)	2497 (58 %)	4342 (100 %)

heat pump system can have a greater advantage if there is an effect that can be obtained through a heat source.

5. Conclusion

In this study, the assessment of clean room heating energy consumption was conducted by selecting CCHPS as a heating equipment. When compared to boilers, CCHPS exhibits advantages in terms of primary energy consumption and carbon emissions. In general buildings, the use of heat pumps is limited due to constraints on heat source utilization. However, in cases like FAB, where significant cooling energy consumption occurs concurrently with heating, the energy-saving effect can be achieved by utilizing the heat source for CHW production. Consequently, CCHPS, with the energy-saving effect incorporated, can achieve a higher heating system COP compared to before the implementation of energy-saving measures. Additionally, it is not advisable to excessively enhance the performance of either the LCHP or HCHP, as that would not be efficient.

The main findings of this study are as follows:

For a CCHPS system with a typical chiller serving as the LCHP, it is recommended to maintain a CW1 temperature of 37 °C when the HCHP absorbs heat from the LCHP condenser. Extreme increase or decrease in the CW1 temperature is not recommended to enhance the performance of either the HCHP or LCHP, as it would not result in energy consumption efficiency improvements for the CCHPS.

By using CCHPS, which obtains heat from a CHW at 17 °C and supplies HW1 at 86 °C, as a heating equipment instead of a boiler, primary energy consumption and carbon emissions can be reduced by 11 % and 25 %, respectively.

Furthermore, unlike boilers, CCHPS produces CHW while supplying heat. This leads to a reduction in the energy consumption by the typical chiller system, resulting in energy-saving effects. Comparing CCHPS with energy-saving measures to boilers, CCHPS reduces primary energy consumption and carbon emissions by 34 % and 44 %, respectively. The heating system COP of CCHPS, with energy-saving measures implemented, improves by 35 % from 2.45 to 3.30.

Future studies will involve obtaining actual OAC operation data to analyze differences with TRNSYS-predicted heating loads and design an appropriate CCHPS system for comparison with the findings of this study.

Funding

This study was supported by grants from the National Research Foundation of Korea (NRF) (No. 2022R1A4A1026503).

CRediT author statement

Taek-Don Kwon: Conceptualization, Methodology, Data curation, Writing original draft preparation. **Woo-Hyun Jeong**: Methodology, Data curation, Validation. **Jae-Weon Jeong**: Supervision, Validation, Reviewing and Editing.

Declaration of competing interest

The authors declare that they have no known competing financial interests or personal relationships that could have appeared to influence the work reported in this paper.

Data availability

Data will be made available on request.

Acknowledgments

The authors gratefully acknowledge Samsung Electronics for providing the necessary facility data and assisting with the system configuration for this study.

Appendix A. Supplementary data

Supplementary data to this article can be found online at https://doi.org/10.1016/j.csite.2023.103745.

References

[1] T.-D. Kwon, J.-W. Jeong, Energy advantage of cold energy recovery system using water- and air-side free cooling technologies in semiconductor fabrication plant in summer, J. Build. Eng. 69 (2023), 106277, https://doi.org/10.1016/j.jobe.2023.106277.

[2] P.C. Slorach, L. Stamford, Net zero in the heating sector: technological options and environmental sustainability from now to 2050, Energy Convers. Manag. 230 (2021), 113838, https://doi.org/10.1016/j.enconman.2021.113838.

[3] O. Ellabban, H. Abu-Rub, F. Blaabjerg, Renewable energy resources: current status, future prospects and their enabling technology, Renew. Sustain. Energy Rev. 39 (2014) 748–764, https://doi.org/10.1016/j.rser.2014.07.113.

[4] D. Gielen, F. Boshell, D. Saygin, M.D. Bazilian, N. Wagner, R. Gorini, The role of renewable energy in the global energy transformation, Energy Strategy Rev. 24 (2019) 38–50, https://doi.org/10.1016/j.esr.2019.01.006.

[5] E. Taibi, D. Gielen, M. Bazilian, The potential for renewable energy in industrial applications, Renew. Sustain. Energy Rev. 16 (2012) 735–744, https://doi.org/10.1016/j.rser.2011.08.039.

[6] C.Y. Lee, S.Y. Huh, Forecasting new and renewable energy supply through a bottom-up approach: the case of South Korea, Renew. Sustain. Energy Rev. 69 (2017) 207–217, https://doi.org/10.1016/j.rser.2016.11.173.

[7] J. Jiang, B. Hu, R.Z. Wang, N. Deng, F. Cao, C.C. Wang, A review and perspective on industry high-temperature heat pumps, Renew. Sustain. Energy Rev. 161 (2022), 112106, https://doi.org/10.1016/j.rser.2022.112106.

[8] J. Jiang, B. Hu, R.Z. Wang, T. Ge, H. Liu, Z. Zhang, Y. Zhou, Experiments of advanced centrifugal heat pump with supply temperature up to 100 °C using low-GWP refrigerant R1233zd(E), Energy 263 (2023) 1–9, https://doi.org/10.1016/j.energy.2022.126033.

[9] H. Liu, B. Zhao, Z. Zhang, H. Li, B. Hu, R.Z. Wang, Experimental validation of an advanced heat pump system with high-efficiency centrifugal compressor, Energy 213 (2020), 118968, https://doi.org/10.1016/j.energy.2020.118968.

[10] J. Shen, G. Feng, Z. Xing, X. Wang, Theoretical study of two-stage water vapor compression systems, Appl. Therm. Eng. 147 (2019) 972–982, https://doi.org/10.1016/j.applthermaleng.2018.11.012.

[11] A. Uusitalo, T. Turunen-Saaresti, J. Honkatukia, J. Tiainen, A. Jaatinen-Värri, Numerical analysis of working fluids for large scale centrifugal compressor driven cascade heat pumps upgrading waste heat, Appl. Energy 269 (2020), 115056, https://doi.org/10.1016/j.apenergy.2020.115056.

[12] S. Boahen, J.M. Choi, A study on the performance of a cascade heat pump for generating hot water, Energies 12 (2019) 1–20, https://doi.org/10.3390/en12224313.

[13] D.H. Kim, H.S. Park, M.S. Kim, Optimal temperature between high and low stage cycles for R134a/R410A cascade heat pump based water heater system, Exp. Therm. Fluid Sci. 47 (2013) 172–179, https://doi.org/10.1016/j.expthermflusci.2013.01.013.

[14] C. Zhang, D. Chai, X. Pan, J. Xie, J. Chen, Performance analysis of two systems combining heat pump and water vapor compression for waste heat recovery, Appl. Sci. 12 (2022), https://doi.org/10.3390/app122412853.

[15] J. Deng, Q. Wei, M. Liang, S. He, H. Zhang, Field test on energy performance of medium-depth geothermal heat pump systems (MD-GHPs), Energy Build. 184 (2019) 289–299, https://doi.org/10.1016/j.enbuild.2018.12.006.

[16] S. Maddah, M. Goodarzi, M.R. Safaei, Comparative study of the performance of air and geothermal sources of heat pumps cycle operating with various refrigerants and vapor injection, Alex. Eng. J. 59 (2020) 4037–4047, https://doi.org/10.1016/j.aej.2020.07.009.

[17] R. Kong, T. Deethayat, A. Asanakham, T. Kiatsiriroat, Performance and economic evaluation of a photovoltaic/thermal (PV/T)-cascade heat pump for combined cooling, heat and power in tropical climate area, J. Energy Storage 30 (2020), 101507, https://doi.org/10.1016/j.est.2020.101507.

[18] G. Xu, S. Deng, X. Zhang, L. Yang, Y. Zhang, Simulation of a photovoltaic/thermal heat pump system having a modified collector/evaporator, Sol. Energy 83 (2009) 1967–1976, https://doi.org/10.1016/j.solener.2009.07.008.

[19] O. Ozgener, Use of solar assisted geothermal heat pump and small wind turbine systems for heating agricultural and residential buildings, Energy 35 (2010) 262–268, https://doi.org/10.1016/j.energy.2009.09.018.

[20] C. Booten, S. Nicholson, M. Mann, O. Abdelaziz, Refrigerants: Market Trends and Supply Chain Assessment, CEMAC Technical Report NREL/TP-5500-70207, 2020.

[21] J. Shen, T. Guo, Y. Tian, Z. Xing, Design and experimental study of an air source heat pump for drying with dual modes of single stage and cascade cycle, Appl. Therm. Eng. 129 (2018) 280–289, https://doi.org/10.1016/j.applthermaleng.2017.10.047.

[22] Korea Meteorological Administration, KMA Weather Data Service, https://data.kma.go.kr/cmmn/main.do. (Accessed 30 June 2023).

[23] D.R. Clark, HVACSIM+ building systems and equipment simulation program reference manual, 84–2996, NBSIR (1985). NIST.

[24] DYNALENE, Dynalene EG technical data sheets. https://www.dynalene.com/wp-content/uploads/2020/06/Dynalene-EG-Tech-Data-Sheet-Rev1.pdf. (Accessed 30 June 2023).

[25] Z. Zhang, H. Qiu, D. Li, Z. He, Z. Xing, L. Wu, Development of ultra-high-efficiency medium-capacity chillers with two-stage compression and interstage vapor injection technologies, Energies 15 (2022) 9562, https://doi.org/10.3390/en15249562.

[26] Z. Janković, J. Sieres, F. Cerdeira, B. Pavković, Analysis of the impact of different operating conditions on the performance of a reversible heat pump with domestic hot water production, Int. J. Refrig. 86 (2018) 282–291, https://doi.org/10.1016/j.ijrefrig.2017.11.005.

[27] KOREAN STANDARDS & CERTIFICATION KS B 6205: LAND BOILERS-HEAT BALANCING. https://standard.go.kr/KSCI/standardIntro/getStandardSearchView.do?menuId=919&topMenuId=502&upperMenuId=503&ksNo=KSB6205&tmprKsNo=KSB6205&reformNo=10. (Accessed 30 June 2023).

[28] Miyawaki, Steam tables. https://www.miyawaki-inc.com/en/technical/table02. (Accessed 30 June 2023).

[29] Ministry of Trade, Industry and Energy of Korea, Enforcement Rules of the Energy Act, 2022. https://www.law.go.kr/. (Accessed 30 June 2023).

[30] KOREA ENERGY AGENCY, Building Energy Efficiency Rating Certification and Zero Energy Building Certification System Operating Regulations, 2022. https://www.energy.or.kr/. (Accessed 30 June 2023).

[31] Greenhouse Gas Inventory & Research Center of Korea, National Greenhouse Gas Emission & Absorption Factor, 2021. http://www.gir.go.kr/home/main.do. (Accessed 30 June 2023).